



HAL
open science

Synchrotron X-Ray Boost Delivered by Microbeam Radiation Therapy After Conventional X-Ray Therapy Fractionated in Time Improves F98 Glioma Control

Marine Potez, Audrey Bouchet, Mélanie Flaender, Claire Rome, Nora Collomb, Michael Grotzer, Michael Krisch, Valentin Djonov, Jacques Balosso, Emmanuel Brun, et al.

► To cite this version:

Marine Potez, Audrey Bouchet, Mélanie Flaender, Claire Rome, Nora Collomb, et al.. Synchrotron X-Ray Boost Delivered by Microbeam Radiation Therapy After Conventional X-Ray Therapy Fractionated in Time Improves F98 Glioma Control. *International Journal of Radiation Oncology, Biology, Physics*, 2020, 107 (2), pp.360-369. 10.1016/j.ijrobp.2020.02.023 . hal-03326708

HAL Id: hal-03326708

<https://hal.science/hal-03326708>

Submitted on 22 Aug 2022

HAL is a multi-disciplinary open access archive for the deposit and dissemination of scientific research documents, whether they are published or not. The documents may come from teaching and research institutions in France or abroad, or from public or private research centers.

L'archive ouverte pluridisciplinaire **HAL**, est destinée au dépôt et à la diffusion de documents scientifiques de niveau recherche, publiés ou non, émanant des établissements d'enseignement et de recherche français ou étrangers, des laboratoires publics ou privés.



Distributed under a Creative Commons Attribution - NonCommercial 4.0 International License

Title: **Synchrotron X-ray boost delivered by Microbeam Radiation Therapy after conventional X-ray therapy fractionated in time improves F98 glioma control**

Short running title: **Synchrotron MRT-Boost for brain tumor**

Marine Potez^{†,=}, Audrey Bouchet^{*,†,=}, Mélanie Flaender[†], Claire Rome^{**,x}, Nora Collomb^{**,x}, Michael Grotzer^{***}, Michael Krisch[^], Valentin Djonov^{*}, Jacques Balosso[†], Emmanuel Brun[†], Jean A. Laissue[§] and Raphaël Serduc[†]

= equal contributor

* Institute of Anatomy, group tomographic and clinical anatomy, University of Bern, Baltzerstrasse 2, CH-3000 Bern 9 Switzerland.

† Rayonnement synchrotron pour la recherche médicale (STROBE), Université Grenoble Alpes, UA7, 71 rue des Martyrs, 38000 Grenoble, France.

** Team Functional NeuroImaging and Brain Perfusion, INSERM U1216, La Tronche, France.

x Grenoble Institut des Neurosciences, Université Grenoble Alpes, La Tronche, France.

§ University of Bern, Hochschulstrasse 4, CH-3012 Bern, Switzerland.

*** Department of Oncology, University Children's Hospital of Zurich, Switzerland.

^ European Synchrotron Radiation Facility, 71 rue des Martyrs, 38000 Grenoble, France.

Corresponding author:

Dr Audrey Bouchet

Rayonnement synchrotron pour la recherche médicale (STROBE), Université Grenoble Alpes, INSERM UA7, 71 rue des Martyrs, 38000 Grenoble, France.

+33 (0)4 76 88 26 37

audrey.bouchet@inserm.fr

Author(s) responsible for statistical analyses:

- Dr Audrey Bouchet

Rayonnement synchrotron pour la recherche médicale (STROBE), Université Grenoble Alpes,
INSERM UA7, 71 rue des Martyrs, 38000 Grenoble, France.

+33 (0)4 76 88 26 37

audrey.bouchet@inserm.fr

- Dr Raphaël Serduc

Rayonnement synchrotron pour la recherche médicale (STROBE), Université Grenoble Alpes,
INSERM UA7, 71 rue des Martyrs, 38000 Grenoble, France.

+33 (0)4 76 88 19 60

serduc@esrf.fr

Conflict of interest notification: none.

Funding statement: The study was supported in France by the ESRF, the Conseil Régional Rhône-Alpes, la Ligue contre le Cancer (comités Drôme et Isère), la Ligue Nationale contre le Cancer, l'Association pour la Recherche contre le Cancer (ARC), the INCA PRTK17048 and ANR-11-LABX-0063/ ANR-11-IDEX-0007.

Acknowledgments

In fond memory of Régine Farion and Elke Bräuer-Krisch who have generously and with heartwarming enthusiasm contributed to this work during so many years. The authors thank Laura Schaad, Andréa Latourre, Warren Aim for technical assistance.

31 **Purpose**

32 Glioblastoma multiforme (GBM) is the most common lethal primary malignancy of the central nervous
33 system (CNS). Radiation therapy with an external beam irradiation is effective against newly diagnosed GBM
34 (1,2). Based on international recommendations, the optimal administered radiation dose is 30 to 35 fractions of
35 1.8 to 2.0 Gy (58 to 60 Gy total dose), 5 days a week. The delivery of 40 Gy as a focal dose to the tumor area,
36 including the surrounding edema, with an additional boost of 20 Gy given to the tumor plus margins, is currently
37 the recommended radiotherapeutic scheme (3). Despite surgical resection and aggressive chemo- and
38 radiotherapy, the prognosis remains very poor: The median survival increases from 5 months to 9 months with
39 adjuvant RT compared to surgery alone (4).

40 Development of a promising new treatment called Microbeam Radiation Therapy (MRT) has been
41 ongoing for the past 25 years. MRT uses synchrotron X-rays collimated into wafers of few tens of microns wide
42 parallel microbeams, separated by a few hundred microns (5,6). This geometry allows a very high dose
43 (hectogray) deposition in the microbeam paths (peak dose) while tissue slices located between microbeams (*i.e.*,
44 in the “valleys”) receive only 5-10% of the peak dose (valley dose) (5,6). Promising experimental results obtained
45 over the last decade have allowed the preparation of veterinary therapeutic trials on pet animals (dogs, cats)
46 bearing spontaneous tumors, for the ultimate evaluation step of MRT efficiency and tolerance on brain tumors
47 before the clinical transfer of MRT. The latter might also be applied after a conventional fractionated irradiation.
48 First preclinical results on technical feasibility and therapeutic relevance of such fractionated MRT have been
49 published (7).

50 Preclinically, few rats survive for a long term after a unique irradiation dose, mainly because the dose
51 required for complete tumor control exceeds normal brain radiotolerance. However, the special irradiation
52 geometry of MRT limits the number of coplanar irradiation ports: The exact patient repositioning required for
53 delivery of successive MRT fractions is impossible because of the submillimetric scale of microbeams. Therefore,
54 it appears rational to combine MRT with conventional multifractionated treatments. Here, the delivery to a brain
55 tumor of only 2 out of 5 fractions in the MRT mode was expected to be more efficient than application of all
56 fractions in the broad beam (BB) mode.

57 Thus, we evaluated the efficiency of MRT delivered after several BB fractions to palliate F98 brain
58 tumors in rats. Tumor volumes were determined by MRI follow-up. The proliferative activity of tumor cells was
59 analyzed using FACS, histological sections, and immunohistology for dynamic changes of the tumor vascular
60 network. Survival curves showed an increase in median survival time (MST) of BB/MRT treated rats compared
61 with BB/BB group, indicating that MRT is a realistic and efficient contribution for brain tumor palliation.

62

63 **Methods and Materials**

64 Procedures related to animal care conformed to the Guidelines of the French Government (licenses
65 380325 and 380321: authorized lab A3818510002 and A3851610004). Rats were anesthetized with a shot of
66 isoflurane 5% in air before maintenance under isoflurane 2.5% for tumor implantation.

67

68 **Tumor inoculation**

69 Ten-week-old (180-220 g) male rats (Fisher344, Charles River laboratories, France) were housed in a
70 controlled environment at 21°C with a day/night cycle of 12 hours, no more than 3 rats per cage; they all had
71 access ad libitum to water and standard laboratory food.

72 F98 glioblastoma cell line was obtained from American Type Culture Collection (ATCC® CRL-2397™,
73 Rockville, MD, USA). The F98 glioblastoma is a tumor model commonly used in neuro-oncology (8); it is poorly
74 vascularized and has an infiltrating profile.

75 F98 cells, p53 mutated (8), were cultured in DMEM (Gibco, 31966-021) supplemented with 10% fetal
76 bovine serum (FBS; Gibco, 16000-036) and 1% penicillin-streptomycin solution (Gibco, 15070-063) in a
77 humidified atmosphere of 5% CO₂ in air. F98 cells were implanted in 83 rats following the protocol described in
78 (7,9) and adapted for F98 cells. Briefly, 10⁶ (5 µl) F98 cells were injected into the right caudate nucleus (3.5 mm
79 from the bregma) at a depth of 5.5 mm below the dura.

80 The number of days elapsed is designated as follows: D_n (after implantation) or T_n (after the first
81 irradiation). The number of rats (n) for each handling are detailed in Figure 1.

82

83 **Magnetic resonance imaging for group sorting; tumor volume measurement**

84 Eight days after F98 implantation, rats underwent anatomical MRI (T₁-weighted image after
85 intraperitoneal (*i.p.*) injection of Gd-DOTA, 200 mg.kg⁻¹ on a Bruker Avance 3 console at 4.7T and volume/surface
86 cross coil configuration (Avance III console; Bruker (Germany); "Grenoble MRI facility IRMaGE,"), to sort them
87 into similar mean tumor volume groups. Rats were divided into a control group (Figure 1); a group of 63 rats
88 irradiated by BB 9, 12, 15 days after tumor implantation, imaged thereafter, then sorted into two groups to be
89 irradiated by 2 additional fractions of either MRT (BB/MRT, n=31) or BB (BB/BB, n=28). A two-way ANOVA with a
90 Sidak post-test was performed with GraphPad 6.0 (significant for p<0.05).

91

92 **Radiation sources and irradiations**

93 ***Conventional exposures on X-ray generator***

94 Conventional orthovoltage irradiations were applied to anesthetized rats, individually, in a PMMA cradle,
95 by a Philips X-ray generator operated at 200 kVp and 20 mA with a 2 mm aluminium inherent filtration. For
96 irradiation of the entire rat's right brain hemisphere, the sagittal suture was positioned on the left side edge of a
97 2.5x2.5 cm² field; the right eye was kept outside of this field. A dose rate of 1.61 Gy/min was determined at the
98 center of the intracerebral tumor using an ionization chamber (Semiflex 31010, PTW). A dose of 6 Gy was

99 delivered to all but control rats at day D₉T₀, D₁₂T₃ and D₁₅T₆. Thereafter the rats of the BB group received a dose
100 of 8 Gy each at D₁₇T₈ and D₁₉T₁₀.

101

102 **MRT exposures**

103 Irradiations at the ID17 biomedical beamline at the European Synchrotron Radiation Facility used an X-
104 rays wiggler source of the 6 GeV electron storage ring, operating at 200 mA. The wiggler produces a wide
105 spectrum of photons which extends, after filtration, from 50 over 350 keV (median energy: 90 keV). The mean
106 dose rate was ~16 kGy.s⁻¹. The quasi-laminar beam was shaped into an array of microscopically thin and quasi-
107 parallel microbeams using a multislit collimator (10). The doses were calculated by means of the Monte Carlo
108 method (detailed dosimetry protocols in (11)). Fifty microbeams, 50 μm wide, spaced 200 μm apart were used.
109 The peak to valley dose ratio was 22.6. The in-microbeam dose was 181 Gy, resulting at tumor depth in an 8 Gy
110 valley dose boost equivalent to that administered by the 2 last BB fractions of the other group. MRT was applied
111 on D₁₇T₈ and D₁₉T₁₀ using two orthogonal and coplanar ports.

112

113 **Treatment evaluation**

114 The survival curves were established using 9 rats for control, 11 for MRT/BB and 15 for BB/BB groups.
115 Three to four rats per groups were imaged at D₁₆T₇, D₂₁T₁₂, D₂₄T₁₅ and D₂₉T₂₀ (Figure 1); their brains were
116 removed for FACS and immunohistological studies.

117

118 **FACS analysis**

119 Freshly dissected brain tumors were mechanically dissociated in 0.05% trypsin. After 5 minutes at 37°C,
120 the cells were flushed, centrifugated, fixed in ice-cold 70% ethanol and kept at -20°C before use. The samples
121 were filtered (Nylon grid 100 μm), rehydrated one night in PBS 1X at 4°C and stained with propidium iodide
122 (5μg.mL⁻¹). Cell cycle distribution was obtained with a BD Accuri C6 Flow Cytometer (Becton Dickinson, USA).
123 Data were treated with FlowJo; statistical analyses were performed in GraphPad 6.0 (t-tests, differences
124 considered as significant for p<0.05). n=4/time/group.

125

126 **Immuno- / histological analyses (IHC)**

127 On 18 μm thick frozen brain sections, Type-IV collagen (C_{IV}), RECA-1 (*Rat Endothelial Cell Antigen*),
128 and glucose receptor-1 (hypoxia reporter) were labeled as previously detailed in (12,13). Proliferating cells were
129 assessed by Ki67 labeling. Using an Olympus fluorescent microscope images and multiple channel mosaics were
130 obtained. n=4/time/group.

131

132 **Quantification**

133 Whole tumor images were quantified using home-made algorithms embedded in the MoreHisto
134 software. Briefly, DAPI stained sections were segmented (watershed with granulometric operator), individualized
135 and counted, leading to the total number of cells in the tumors. Ki67 (red staining) was also segmented using

136 Otsu threshold; tumor cells were considered as positive for Ki67 when at least 80% of DAPI+ pixels in the nucleus
137 contained Ki67 staining. Ratios of Ki67+/DAPI+ were determined for each tumor. In a second time, we estimated
138 for each DAPI cell the number of Ki67+ cells located in a 200 μ m radius circle around the considered cells.
139 Percentage of DAPI+ cells with n Ki67+ cells in this region are reported in figure 4. C_{IV}, RECA-1 and GLUT1
140 staining were segmented separately; vessels were counted when they expressed 3 biomarkers. Differences in
141 vessel density, diameters and inter-vessel distances were evaluated using t-tests on GraphPad 6.0.

142

143 **Results**

144

145 **MRT-Boost stops F98 tumor growth and increases the lifespan of rats bearing intracranial F98 more than**
146 **BB irradiation alone**

147 Figure 2 and 3A show representative F98 tumors on T₁-weighted MR images at different times after
148 treatment, and the corresponding lesion volumes. Untreated F98 tumors grew exponentially between D₈T₋₁ and
149 D₂₄T₁₅, reaching a volume of 696.4 ± 66.9 mm³. On T₇, tumor volumes were significantly lower after the 3 fractions of
150 6 Gy BB, compared with controls. (p<0.001). On T₁₅, unirradiated tumors were 3.8 times larger than BB-treated tumors
151 (p<0.001). At the same time, the mean volume of tumors exposed to two MRT fractions of 8 Gy was about half of those
152 irradiated by two BB fractions (8 Gy each) (89.9±36.0 and 181.4±84.5 mm³ respectively, p<0.0001). Despite two other
153 8 Gy fractions, BB irradiated tumors recurred and grew exponentially. Significant differences occurred in the BB/BB group
154 between T₇ and T₂₅ (p<0.001). Conversely, 2 fractions of MRT stopped tumor growth: no differences in tumor size were
155 found in the BB/MRT group between T₇ and T₂₅ (Figure 3A). Moreover, the tumors irradiated with BB/MRT tended to
156 shrink between T₁₂ and T₁₅, but the difference was not significant (p=0.0633) (Suppl fig. 1).

157 Figure 3B shows the survival curves of untreated, BB/BB and BB/MRT-treated, F98 bearing rats. BB/BB
158 significantly increased the MST (Mean Survival Time) of irradiated rats (T₂₆) versus non-irradiated control rats
159 (T₁₅, p<0.0001). MRT fractions further increased MST: survival times were significantly higher (p=0.0144) in the
160 BB/MRT group (T₃₃) compared with those in the BB/BB group. Increases in lifespan were 73.3% and 120% for BB
161 and MRT groups, respectively.

162

163 **MRT-Boost reduces proliferative index of F98 tumors and modifies cell cycle distribution**

164 Representative mosaics of whole irradiated tumors in Figure 4, column A, show Ki67 (red) and DAPI
165 (blue) immuno-labelling of control tumors (Ctrl) and tumors irradiated at T₇.

166 The quantification in Figure 4, column B, shows the percentageKi67+ cells (within a 200 μm radius
167 circle, column C) with t-test results. The 3x6 Gy BB exposures (B, first row) reduced the proliferative index of F98
168 tumors, versus control values (Ki67+/DAPI ratio). Two additional MRT fractions led to a marked decrease of the
169 proliferative index, from T₁₂ to T₂₀ after irradiation, compared with 2 supplemental BB fractions; these reductions
170 reached significant differences at T₁₂ and T₂₀ (p=0.0041 and 0.018, respectively).

171 Figure 4, column C, represents the percentage of DAPI cells that are surrounded by the number (n) of
172 Ki67+ cells within a 200 μm radius circle, with t-test results. First row: On day 7, in the CTRL group, half of tumor
173 cells are neighbored by 48±17 Ki67+ cells (dashed curve). The irradiation of F98 tumors by 3X6 Gy reduced their
174 number to 27±20 Ki67+ cells (black curve). Column C, three lower rows: MRT fractions reduced the number of
175 neighboring proliferative cells significantly compared with BB fractions. Indeed, in the MRT group the number of
176 adjacent proliferative cells remained constant between T₁₂ (second row) and T₂₀ (bottom row), whilst the number
177 of vicinal cells increased from 15±6 to 74±14 cells in the BB group. These data reflect tumor recurrence with high

178 proliferation hot spots within BB irradiated tumors, while a MRT-Boost significantly controls tumor
179 aggressiveness.

180 Figure 4, column D: Cell cycle distribution analysis obtained by flow cytometry showed that after the
181 3x6 Gy irradiation, the number of G1 cells increased, whereas S and G2/M cell fractions decreased at T₇
182 compared with the non-irradiated group (p<0.01, 0.01 and 0.05 respectively, first row).

183 At T₁₅ (third row), G1 cells increased markedly after MRT-Boost, but minimally after BB irradiation
184 compared to the T₇ values. Significant differences in the fraction of cells in G1 and G2/M between BB/MRT and
185 BB/BB groups were measured on T₂₀ (bottom row): BB/BB displayed a cell cycle distribution similar to that of non-
186 treated tumors on T₇. At T₂₀, in both BB/MRT and BB/BB groups, the fraction of cells in G1 phase returned to
187 values like those of non-irradiated control tumors on T₇. Conversely, the fraction of S phase cells differed
188 significantly between BB/MRT and BB/BB groups (p<0.05).

189

190 **MRT-Boost induces minor changes in tumor vascular morphometric parameters**

191 Representative images of whole irradiated tumors in Figure 5A show ReCa-Coll-IV-Glut1 triple immuno-stained
192 vessels 7, 12, 15 and 20 days after the start of treatment. There was no significant difference in vessel density (percentage
193 of vascular surface, Figure 5B), nor vascular tortuosity (data not shown) between the 2 combinations of irradiation. Only
194 tumors irradiated with 3x6 Gy showed a significant decreased of inter-vessel half distance compared to sham irradiated
195 tumors (last column). Vascular diameters were not modified, except at day 12 (Figure 5B second row) when diameters of
196 tumor vessels irradiated by MRT were significantly lower than of those irradiated by BB ($11.095\pm 0.152\ \mu\text{m}$ vs
197 $8.284\pm 0.542\ \mu\text{m}$, p=0.0077 (t-test).

198

199

200 **Discussion**

201

202 Temporal fractionation is the clinical standard radiotherapy protocol applied to high grade brain tumors.
203 Attempts of improving treatment efficiency (hyper, hypofractionation, local boost...) led to modest increases in
204 patient lifespans (14). MRT, a novel concept of spatially fractionated radiotherapy based on the high photon flux
205 of synchrotron-generated X-rays, has been proposed as promising treatment concept for patients with malignant
206 brain tumors for whom no satisfactory therapy is available yet (15). The therapeutic effects of microbeam arrays
207 were mainly studied in laboratory rats and chick chorioallantoic membranes after a single radiation dose
208 (6,13,16–21). Only one trial of temporal MRT fractionation has been conducted at the ESRF (7). Here, we
209 demonstrate that MRT can increase radiotherapeutic efficiency when delivered as boost after a temporally
210 fractionated conventional treatment. Indeed, MRT completely stopped tumor growth during ~4 weeks and
211 significantly increased MST while BB-tumors recurred within few days after the last radiation fraction.

212

213 Two MRT fractions, given after 3 fractions of 6Gy BB, modified tumor cell proliferation and cell cycle
214 characteristics to a larger extent than 2 BB fractions did, albeit MRT delivered the same valley dose as the BB.
215 The choice of the conditions for comparison of MRT with other radiation therapies modalities is complex due to
216 the specificities of MRT (high dose rate, single irradiation session, periodical spatial alternation of microscopic
217 dose distribution, *i.e.*, of peak and valley doses). Several solutions have been proposed for a dosimetric
218 conversion, among others, the use of the integrated MRT dose. In the configuration used in this study (50 μm
219 beam width, 200 μm center-to-center spacing), the integrated/average dose is around 55 Gy for the MRT group
220 (peak dose: 181 Gy). This integrated dose was calculated by the Monte Carlo Method for the peak and valley
221 doses. Integrated doses was also measured with current dosimeters, since a very high spatial resolution of peak
222 and valley doses is not necessary in this configuration. Application of high doses such as 55 Gy by large
223 homogenous fields of conventional irradiation to a rat brain is not rational since they destroy normal brain tissue
224 and cause the animal's death. Therefore, we did not apply them in animal experiments, for biological and ethical
225 reasons. The valley dose of MRT was chosen as a point of comparison between the two geometries of irradiation
226 in the current study, as it was the case in previous paper (19). This choice was reinforced by the fact that the
227 valley area in MRT represented the largest fraction (75%) of irradiated tissue. To use a BB dose equal to the
228 valley dose in MRT has been shown in many published preclinical experiments to better reflect the biological
229 impact than using the integrated dose. However, the biological impact of such MRT versus BB irradiations differs.
230 This difference is most likely due to the presence of the microbeam peaks. There is little doubt that the presence
231 of those peaks enhances the tumor control by MRT compared to that achieved by BB at equal valley dose,
232 because of the additional dose deposition. It is predictable that selectively increased BB doses could increase the
233 tumor control to the same level of control obtained by MRT, but the toxicity on normal brain would increase
234 disproportionately because of the coincident delivery of the BB dose to the normal tissues. Bouchet *et al.* 2016
235 (19) observed that MRT with a peak dose of 200 Gy had a similar impact on animal survival, compared to the BB
236 group, while the MRT valley dose (75% of the irradiated area) was 2 times smaller than the homogeneous dose

237 applied in BB mode. Moreover, these considerations refer to a unidirectional application of MRT; recent data of
238 our group, submitted for publication, show that multidirectional (multiport) MRT (with its lower valley dose also
239 used for BB) produces unexpectedly high biological equivalent dose factors (up to x2.5), while warranting a very
240 high tolerance for normal tissues in the trajectory of the individual arrays.

241 Another concern relates to the fact that current MRT beams are orthovoltage X-rays in the order of 100
242 keV. The depth of penetration of those beams is relatively low, and they are heavily absorbed by bone. However,
243 the falloff of dose with increasing depth in tissue is considerably more gradual in the valleys than in the peaks
244 (22). Typically, a half dose attenuation is obtained at 4.5 cm (median energy 90 keV), but the superior benefits of
245 MRT still prevail under these conditions. Moreover, the ultimate intention is to use multidirectional arrays focused
246 on the target region, and to treat brain tumors in children where the attenuation is weaker than in the head of
247 adults.

248

249 The MRT boost significantly prolonged the G0/G1 cell arrest observed after the first set of BB
250 exposures, but the two last BB fractions did not (Figure 4). At T₁₅, *i.e.*, 3 days after the last irradiation, cell cycle
251 distribution in the BB/BB group was similar to that in the control group, while the effects of radiation persisted in
252 the BB/MRT group; and while S and G2/M phase populations significantly decreased. Conversely, the association
253 of BB and MRT completely stopped tumor growth during more than one month. A treatment completion using
254 only conventional X-ray beams did not prevent tumor recurrence. Changes in cell cycle redistribution induced by
255 MRT were combined with other histopathological events: the Ki67/DAPI ratio was significantly reduced after MRT
256 Boost compared with BB alone, whatever the time after irradiation. Most of the vascular parameters were not
257 significantly modified after MRT (Figure 5). MRT is known to have damaged immature vascular networks of
258 zebrafish (23) and of other tumor models (review: (18)). The hypo-vascularization (blood volume fraction (BVf):
259 ~2%) of the F98 model may prevent vascular effects as those seen in the high BVf (>5%) 9L model (9).

260 Experimental findings strongly support the clinical evaluation of cell cycle inhibitors in combination with
261 radiation. For instance, a new chalcone, the microtubule polymerization inhibitor JAI-51, was administered alone
262 or immediately after MRT to rats bearing intracerebral gliosarcomas. MRT plus JAI-51 – but not JAI-51 alone -
263 increased significantly the lifespan compared with MRT alone ($p=0.0367$). MRT alone or associated with JAI-51
264 induced a cell cycle blockade in G2/M ($p<0.01$) while the combined treatment also reduced the proportion of
265 G0/G1 cells. MRT and JAI-51 combined increased the survival of 9LGS-bearing rats by inducing
266 endoreduplication of DNA and tumor cell death and delayed the onset of tumor growth resumption two weeks
267 after treatment (16). Further, G2 checkpoint abrogators, such as Wee kinase inhibitors, have been shown to
268 enhance cell killing of conventional cancer radiotherapy through the induction of premature mitosis (24).
269 Nanomolar concentrations of MK-1775, another potent and selective wee1 kinase inhibitor, radiosensitized
270 human p53-defective human lung, breast, and prostate cancer cells but not similar lines with wild-type p53,
271 abrogating the radiation induced G2 block in p53-defective cells but not in p53 wild-type lines. MK-1775 also
272 significantly enhanced the anti-tumor efficacy of radiation *in vivo* against p53-defective tumors (25).

273 In previous studies, MRT was more efficient than BB for controlling brain tumors such as 9L gliosarcoma
274 (19) or F98 glioblastoma (20). BB doses 3 times higher than MRT doses were necessary for F98 tumor control
275 and prolongation of MST (20). A single BB fraction of 15 Gy (calculation performed with LQL-Equiv. software.
276 equivalent radiation dose in 2 Gy fractions (EQD2 31.3 Gy)), delivered to F98 bearing rats, led to an increase in
277 lifespan (ILS) of 15% (26). Likewise, in this study, MRT delivered after temporally fractionated BB irradiation was
278 more efficient than equivalent BB irradiation (Figure 3) and yielded significantly longer MST (T_{33} versus T_{26}) and
279 ILS (120% versus 73%) for the BB/MRT group than for BB/BB group. MRT increased MST compared with BB to
280 a larger extent after temporal fractionation. Yang *et al.* (27) have delivered EQD2 of 25 Gy (5x4 Gy) to F98
281 tumors and obtained an ILS of 17.4%. Previous work showed that a unique fraction of MRT with a valley dose of
282 18 Gy led to a 52-63% ILS (19). In the present study, an ILS of 120% was obtained after similar MRT valley
283 doses of 16 Gy delivered after temporally fractionated BB; EQD2 were 42 and 47.6 Gy, respectively (calculation
284 performed with LQL-Equiv. software). A lower ILS (100%) was also obtained for a 10x4 Gy (daily fractions) on the
285 same tumor model and a similar equivalent EQD2 (46.5 Gy) (19). Optimization of prescribed dose, fractionation
286 scheme and treatment plan for an improved therapeutic index of BB/MRT combined radiotherapy are
287 indispensable for a clinical transfer of MRT in the next years. Patients cannot be re-positioned with micrometer
288 precision for treatment delivery thus preventing daily re-irradiation through the same incidences. It appears that
289 MRT will be, at first, used as a boost or a smaller part of a standardized treatment, then progressively adapted as
290 integrated part of a standardized treatment. Current experiments on large animals will consolidate our
291 understanding of MRT's radiobiological long-term effects on normal tissues and prepare the safe clinical transfer
292 for brain tumor bearing patients.

293

294 This study shows for the first time that MRT, delivered as a boost completing a conventional fractionated
295 irradiation by orthovoltage broad X-ray beams, is feasible and more efficient than a boost in the conventional
296 radiotherapy mode. The translation of MRT from the preclinical stage to a Phase I human clinical trial may be
297 achieved after (1) a successful veterinary phase I/II trial for pet animal patients (cats and dogs) bearing
298 spontaneous tumors, as they provide a good link between tumor models in animals and humans with regard to
299 tumor size and irradiation fields; (2) the development and validation of a MRT-specific treatment planning system
300 and a new patient positioning system; (3) selected preclinical studies to complement the most recent technical
301 developments and to answer some remaining questions. These endeavors are being pursued by our
302 collaborative team with the objective of using microbeams for a first human patient in 3 to 4 years.

303

304

305

306

307

308 **Figure 1: Experimental design.** Tumor inoculation, MRI session for size sorting (white rectangle, dashed), MRI
 309 session (white rectangles), broad beam irradiation (black and grey rectangles), MRT (green rectangles), tissue
 310 sampling and analysis (crossed circle). Days after inoculation (D) and treatment (T); n designates the number of
 311 animals.

312
 313 **Figure 2: MRI follow up of irradiated F98 tumors.** A- T_1 -weighted MR imaging: Non-irradiated (CTRL), BB/BB
 314 and BB/MRT-treated tumors in rat brain at different times after implantation and treatment. B- Example of tumor
 315 on hematoxylin/eosin staining tissue horizontal sections 9, 18, 23, 26, 31 days after tumor inoculation (D) *i.e.* -1, 7,
 316 12, 15, 20 days after the first irradiation (T).

317
 318 **Figure 3: MRT-Boost stops F98 tumor growth and improves survival of F98 tumor bearing rats.** A- Means
 319 of tumor volume measured on T_1 -weighted images for sham (black), BB/BB (grey) and BB/MRT (green)-irradiated
 320 groups. Mean \pm SEM. 2-way ANOVA with Sidak post test. *, **, ***, ****: significantly different from time matched
 321 analysis, $p < 0.05$, 0.01, 0.001, 0.0001, respectively. B- Kaplan Meier survival curves of untreated (CTRL, dashed),
 322 treated by BB/BB (grey) and BB/MRT (green). Table: significant differences between groups (log-rank test).

323
 324 **Figure 4: MRT-Boost reduces tumor proliferation index.** A- Representative merged mosaics of an entire
 325 tumor immunostained with Ki67 (red) and DAPI (blue). First row: untreated group (Ctrl) and 3x6 Gy BB fractions
 326 on T_7 . Three lower rows: BB/BB (+2x8 Gy BB fractions) and BB/MRT (+2x8 Gy MRT fractions). B- Ki67 positive
 327 cells/DAPI cells ratio quantified on whole tumors 7, 12, 15 and 20 days after treatment. Control, 3x6 Gy BB (in
 328 first row only), BB/BB and BB/MRT groups (in three lower rows) are represented as light grey dots, black
 329 squares, grey hexagons and green triangles respectively; p-values for t-test comparisons. C- Percentage of DAPI
 330 cells that are surrounded by the number (n) of Ki67+ cells within a 200 μ m radius circle, with t-test results. D-
 331 FACS analysis of cell cycle distributions of tumor cells in untreated controls (black dot pattern), after 3x6 Gy BB
 332 (black), BB/BB (grey) and BB/MRT (green) groups 7, 12, 15 and 20 days after treatment start. *, **: significantly
 333 different values from those of time matched group(s) within the same cycle phase. $p < 0.05$ and 0.01 t-test values:
 334 +, ++, respectively. Ctrl versus T_7 irradiated groups (3x6 Gy), significantly different t-test values of $p < 0.05$ and
 335 0.01, respectively: ^, ^^.

336
 337
 338 **Figure 5: MRT-Boost does not modify F98 vascular network.** A- Representative merged mosaics of an entire
 339 tumor immunostained with Glut-1 (green), Reca-1 (red) and Collagen IV (blue) for control group, after 3x6 Gy BB
 340 fractions, BB/BB (+2x8 Gy BB fractions) and BB/MRT (+2x8 Gy MRT fractions). B- Vessels percentage surface
 341 (first row), diameter (second row), and inter-distance (third row), of tumor vessels of F98 bearing rats 7, 12, 15
 342 and 20 days after treatment start. Untreated (Ctrl), treated group by 3x6 Gy BB fractions, BB/BB (+2x8 Gy BB
 343 fractions) and BB/MRT (+2x8 Gy MRT fractions) are represented in black dot pattern, black, grey and green
 344 histograms respectively. **: $p < 0.01$ (t-test).

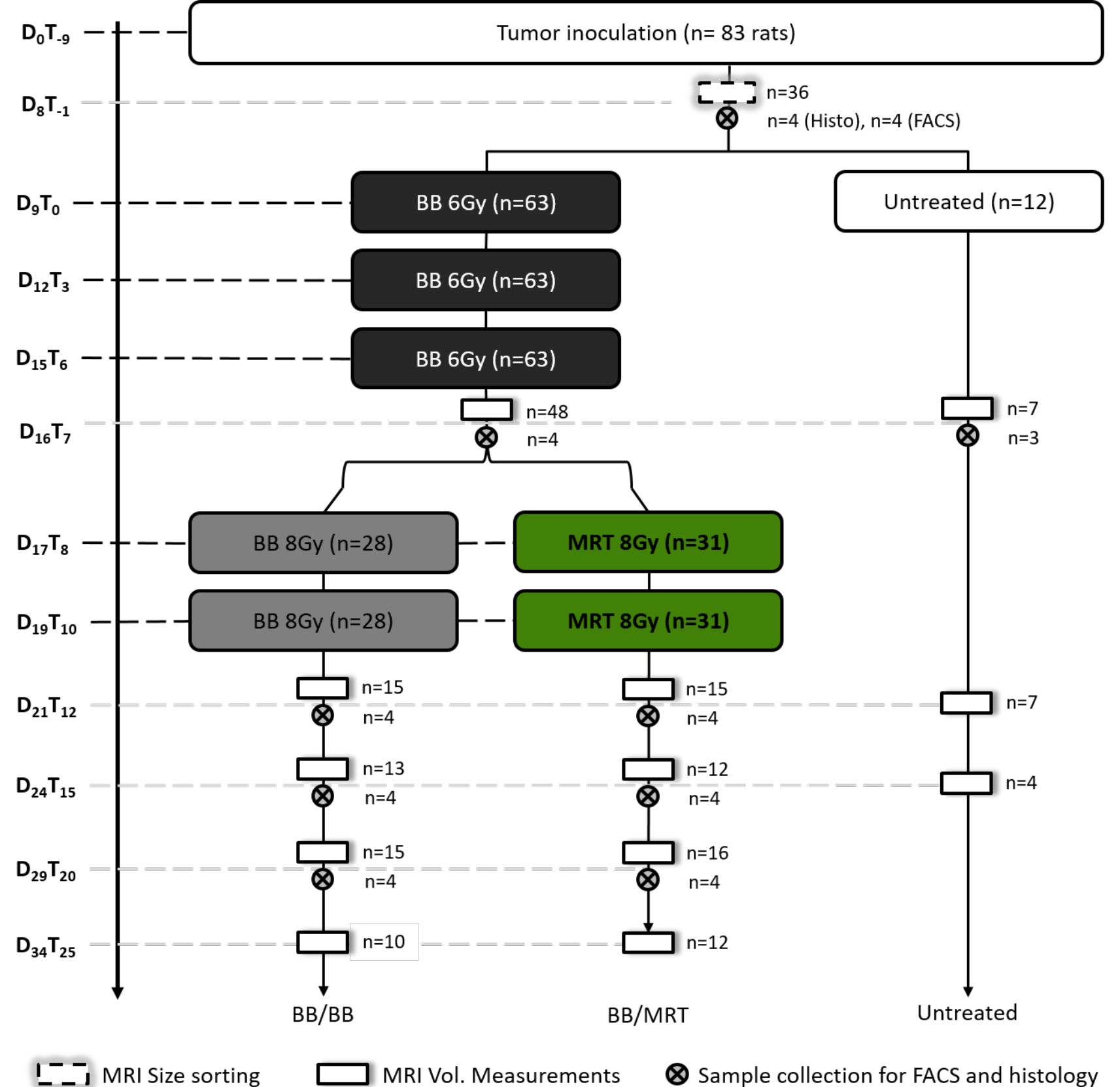
345

346 **References**

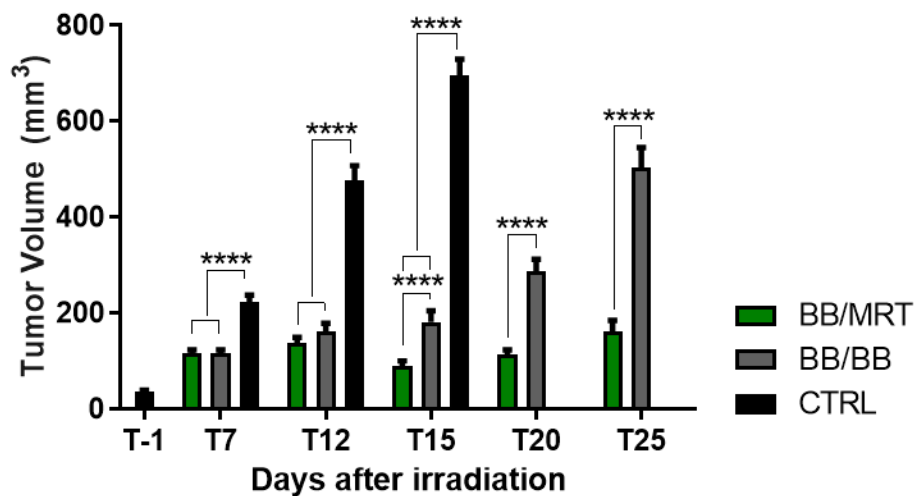
- 347 1. Andersen AP. Postoperative irradiation of glioblastomas. Results in a randomized series. *Acta Radiol*
 348 *Oncol Radiat Phys Biol* [Internet]. 1978 [cited 2014 Jul 14];17:475–84. Available from:
 349 <http://www.ncbi.nlm.nih.gov/pubmed/216238>
- 350 2. Walker MD, Alexander E, Hunt WE, MacCarty CS, Mahaley MS, Mealey J, et al. Evaluation of BCNU
 351 and/or radiotherapy in the treatment of anaplastic gliomas. A cooperative clinical trial. *J Neurosurg*
 352 [Internet]. 1978 [cited 2014 Jul 14];49:333–43. Available from:
 353 <http://www.ncbi.nlm.nih.gov/pubmed/355604>
- 354 3. Garden AS, Maor MH, Yung WK, Bruner JM, Woo SY, Moser RP, et al. Outcome and patterns of failure
 355 following limited-volume irradiation for malignant astrocytomas. *Radiother Oncol* [Internet]. 1991 [cited
 356 2014 Jul 14];20:99–110. Available from: <http://www.ncbi.nlm.nih.gov/pubmed/1851573>
- 357 4. Walker MD, Green SB, Byar DP, Alexander E, Batzdorf U, Brooks WH, et al. Randomized comparisons
 358 of radiotherapy and nitrosoureas for the treatment of malignant glioma after surgery. *N Engl J Med*
 359 [Internet]. 1980 [cited 2014 Jul 14];303:1323–9. Available from:
 360 <http://www.ncbi.nlm.nih.gov/pubmed/7001230>
- 361 5. Slatkin DN, Spanne P, Dilmanian FA, Sandborg M. Microbeam radiation therapy. *Med Phys*.
 362 1992;19:1395–400.
- 363 6. Brauer-Krisch E, Serduc R, Siegbahn EA, Le Duc G, Prezado Y, Bravin A, et al. Effects of pulsed,
 364 spatially fractionated, microscopic synchrotron X-ray beams on normal and tumoral brain tissue. *Mutat*
 365 *Res*. 2009/12/26. 2010;704:160–6.
- 366 7. XXXX_Blinded_author_details_XXXX
- 367 8. Barth RF. Rat brain tumor models in experimental neuro-oncology: the 9L, C6, T9, F98, RG2 (D74), RT-2
 368 and CNS-1 gliomas. *J Neurooncol* [Internet]. 1998 [cited 2016 Dec 26];36:91–102. Available from:
 369 <http://www.ncbi.nlm.nih.gov/pubmed/9525831>
- 370 9. XXXX_Blinded_author_details_XXXX
- 371 10. Bräuer-Krisch E, Requardt H, Brochard T, Berruyer G, Renier M, Laissue JA, et al. New technology
 372 enables high precision multislit collimators for microbeam radiation therapy. *Rev Sci Instrum* [Internet].
 373 2009 [cited 2013 Jan 31];80:074301. Available from: <http://www.ncbi.nlm.nih.gov/pubmed/19655968>
- 374 11. Martínez-Rovira I, Sempau J, Prezado Y, Martínez-Rovira I. Monte Carlo-based treatment planning
 375 system calculation engine for microbeam radiation therapy. *Med Phys* [Internet]. 2012 [cited 2013 Sep
 376 17];39:2829–38. Available from: <http://www.ncbi.nlm.nih.gov/pubmed/22225281>
- 377 12. XXXX_Blinded_author_details_XXXX
- 378 13. XXXX_Blinded_author_details_XXXX
- 379 14. von Neubeck C, Seidlitz A, Kitzler HH, Beuthien-Baumann B, Krause M. Glioblastoma multiforme:
 380 emerging treatments and stratification markers beyond new drugs. *Br J Radiol* [Internet]. 2015 [cited 2019
 381 Jul 23];88:20150354. Available from: <http://www.ncbi.nlm.nih.gov/pubmed/26159214>
- 382 15. Laissue JA, Blattmann H, Wagner HP, Grotzer MA, Slatkin DN. Prospects for microbeam radiation
 383 therapy of brain tumours in children to reduce neurological sequelae . *Dev Med Child Neurol*.
 384 2007;49:577–81.
- 385 16. XXXX_Blinded_author_details_XXXX
- 386 17. XXXX_Blinded_author_details_XXXX
- 387 18. XXXX_Blinded_author_details_XXXX
- 388 19. XXXX_Blinded_author_details_XXXX
- 389 20. XXXX_Blinded_author_details_XXXX
- 390 21. XXXX_Blinded_author_details_XXXX

- 391 22. Slatkin DN, Blattmann H, Wagner HP, Glotzer MA, Laissue JA. "Prospects for microbeam radiation
392 therapy of brain tumours in children." *Dev. Med. Child Neurol.* 2009. page 163.
- 393 23. Brönnimann D, Bouchet A, Schneider C, Potez M, Serduc R, Bräuer-Krisch E, et al. Synchrotron
394 microbeam irradiation induces neutrophil infiltration, thrombocyte attachment and selective vascular
395 damage in vivo. *Sci Rep [Internet]*. 2016 [cited 2016 Dec 19];6:33601. Available from:
396 <http://www.ncbi.nlm.nih.gov/pubmed/27640676>
- 397 24. Wang Y, Li J, Booher RN, Kraker A, Lawrence T, Leopold WR, et al. Radiosensitization of p53 mutant
398 cells by PD0166285, a novel G2 checkpoint abrogator. *Cancer Res.* 2001;61:8211–7.
- 399 25. Bridges KA, Hirai H, Buser CA, Brooks C, Liu H, Buchholz TA, et al. MK-1775, a novel Wee1 kinase
400 inhibitor, radiosensitizes p53-defective human tumor cells. *Clin Cancer Res [Internet]*. 2011 [cited 2020
401 Jan 10];17:5638–48. Available from: <http://www.ncbi.nlm.nih.gov/pubmed/21799033>
- 402 26. Bobyk L, Edouard M, Deman P, Rousseau J, Adam J-F, Ravanat J-L, et al. Intracerebral delivery of
403 Carboplatin in combination with either 6 MV Photons or monoenergetic synchrotron X-rays are equally
404 efficacious for treatment of the F98 rat glioma. *J Exp Clin Cancer Res [Internet]*. 2012 [cited 2017 Apr
405 25];31:78. Available from: <http://www.ncbi.nlm.nih.gov/pubmed/22992374>
- 406 27. Yang Y, Crosbie JC, Paiva P, Ibahim M, Stevenson A, Rogers PAW. In vitro study of genes and
407 molecular pathways differentially regulated by synchrotron microbeam radiotherapy. *Radiat Res*
408 *[Internet]*. 2014 [cited 2015 May 24];182:626–39. Available from:
409 <http://www.ncbi.nlm.nih.gov/pubmed/25409126>

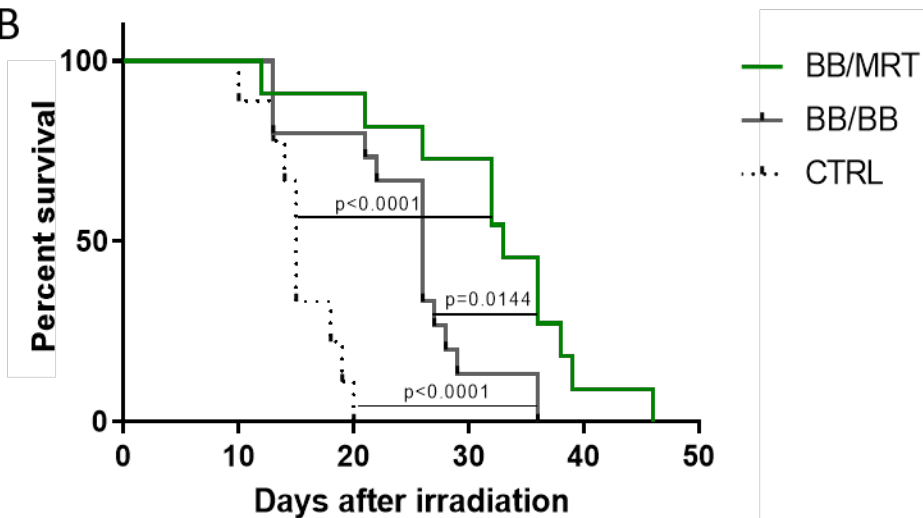
410

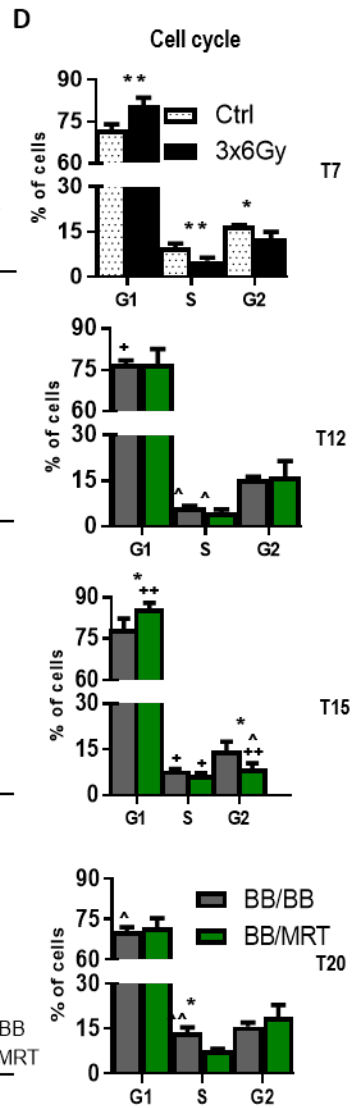
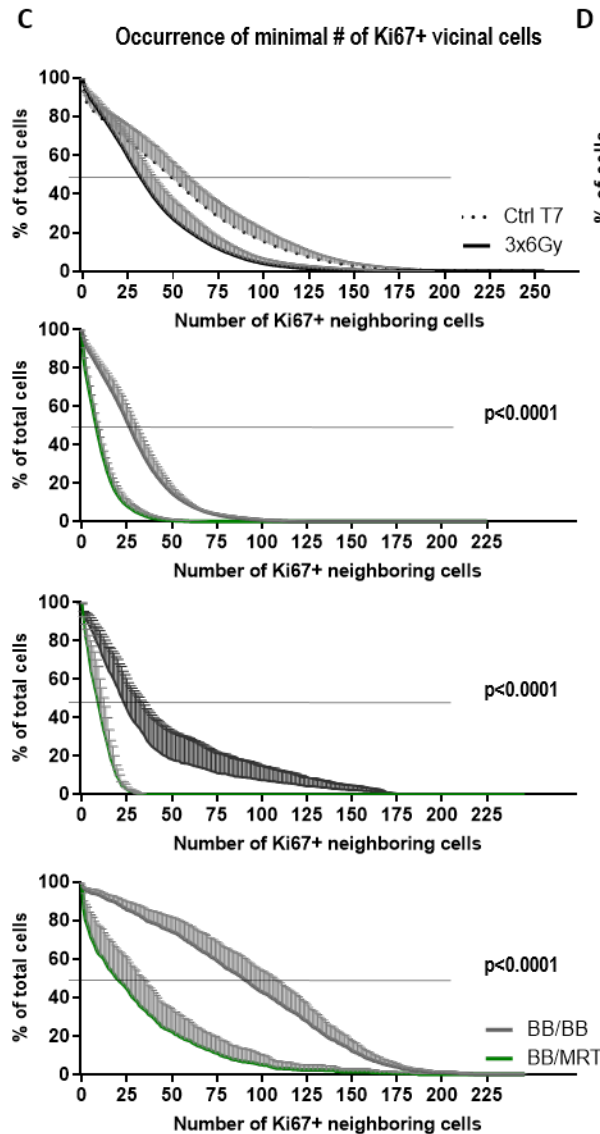
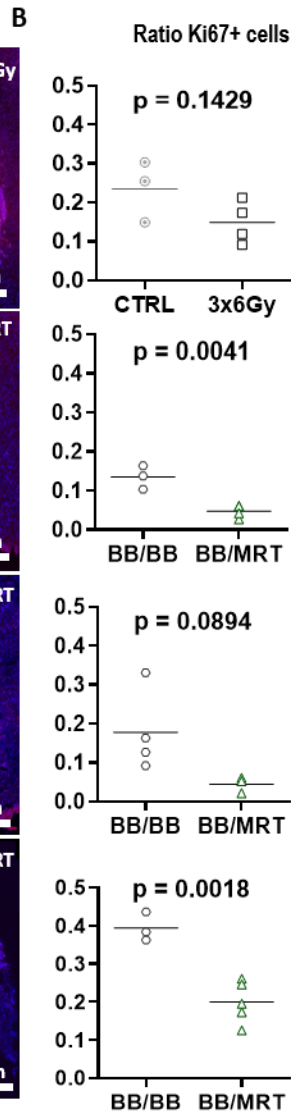
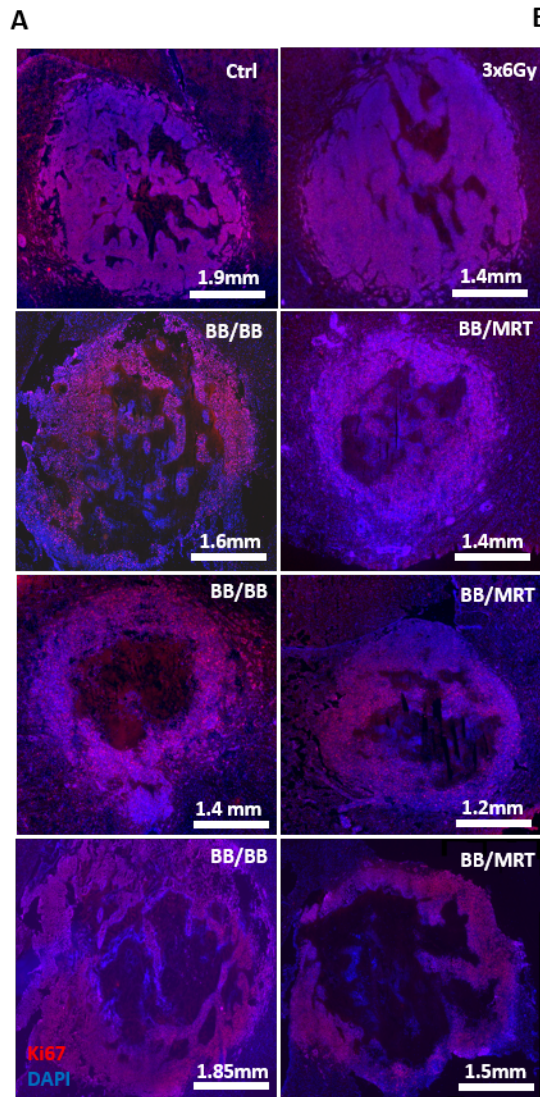


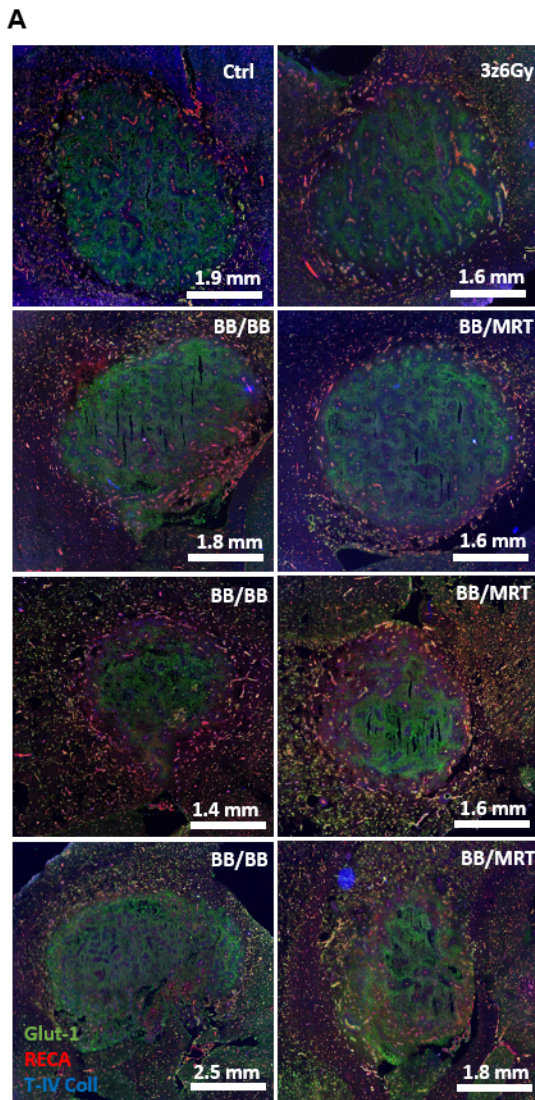
A



B







B

			Vascular surface (%)	Vessels diameter (μm)	Vascular 1/2 distance (μm)
T7	CTRL	Mean	0.833	6.859	54.353
		SD	0.252	1.034	5.572
	3x6Gy	Mean	1.275	8.800	42.538
		SD	0.896	1.427	6.129
T-test		p value	0.454	0.105	0.047

T12	BB/BB	Mean	1.833	11.095	50.383
		SD	0.503	0.263	4.488
	BB/MRT	Mean	1.200	8.284	47.644
		SD	0.535	1.084	10.803
T-test		p value	0.174	0.008	0.702

T15	BB/BB	Mean	2.175	10.621	50.774
		SD	1.164	1.936	26.693
	BB/MRT	Mean	2.100	10.245	53.280
		SD	1.010	1.824	10.171
T-test		p value	0.926	0.787	0.866

T20	BB/BB	Mean	1.450	8.309	47.935
		SD	0.480	0.861	10.151
	BB/MRT	Mean	1.450	7.818	45.190
		SD	0.520	0.652	3.542
T-test		p value	>0.999999	0.397	0.628